Electron-spin-resonance study of electron properties in nitrogen and carbon austenites

V. G. Gavriljuk, S. P. Efimenko, Ye. E. Smuk, and S. Yu. Smuk

Institute of Metal Physics, Ukraine Academy of Science, Kiev, Ukraine

B. D. Shanina, N. P. Baran, and V. M. Maksimenko

Institute of Semiconductors, Ukraine Academy of Science, Kiev, Ukraine

(Received 3 June 1992; revised manuscript received 14 December 1992)

Electron-spin resonance was studied in the $Cr_{21}Ni_{16}Mn_7$ and $Cr_{20}Ni_{16}Mn_6$ austenites with different content of nitrogen and carbon. Measurements were made in the temperature region 10–300 K. Temperature dependences were obtained for the absorption-derivative signal parameters such as the intensity $I(T)$, the width $\Delta H(T)$, and the asymmetry parameter $R(T)$. Theoretical analysis of the signal shape revealed that its temperature dependence is equivalent to its dependence on the inverse length of electron diffusion δ_e through the skin layer δ, if the value $(\delta\delta_e)$ is constant while the temperature changes. The dependence of the electron-state density on the Fermi surface $D(\varepsilon_F)$ upon the solutes content is deduced from the fitting of theoretical and experimental curves $I(T)$, $\Delta H(T)$, and $R(T)$. It was established that $D(\varepsilon_F)$ increases in nitrogen austenite and decreases in carbon austenite with the growth of nitrogen and carbon concentration.

I. INTRODUCTION

As interstitial solutes, nitrogen and carbon extensively affect the mechanism and the kinetics of structural and phase transformation in iron-based alloys, specifically, the creation of the high-temperature iron γ phase named austenite. Electrical and mechanical properties of austenite depend on the distribution of nitrogen and carbon atoms in solid solution. As an alloying element in the austenite nitrogen enables to solve the problem of the strengthening of stainless steels. Nitrogen and carbon austenites differ as to their mechanical properties such as strength, fracture toughness, wear resistance, etc.[1,2] Nitrogen and carbon austenites differ in thermal stability, possibly on account of the different distribution of doped atoms in solid solution. The effects of nitrogen and carbon on the stacking-fault energy in γ iron are opposite.[3,4] The reasons for the above-mentioned difference are not clear yet but presumably they could be found in the different hybridization of valence orbitals and the differing contributions to states density on the Fermi surface of these alloys.

The technique of electron-spin resonance (ESR) was applied to look into this question. The ESR method is traditionally used in the physics of solid state to study localized electron properties. A large number of papers has been dedicated to the study of conduction electron-spin resonance (CESR) in pure metals[5–12] and Cu-Mn alloys.[13,14] We used CESR in Refs. 15 and 16 to study paramagnetic alloys based on other transient d metals (Cr,V,Ni).

The CESR intensity in metals is proportional to the electron-state density on the Fermi surface $D(\varepsilon_F)$ and its study may be a suitable way to research the effects of different technology factors on the $D(\varepsilon_F)$. Unfortunately the observation of CESR is not always possible. Specifically, the magnetic ordering in the d-element alloys usually makes CESR unobservable. Austenites are paramagnetic alloys, and that is why they can be studied by means of the CESR method.

In this study we made temperature measurements of the CESR signal parameters and performed a detailed theoretical analysis of the absorption-derivative signal shape taking into account the anomalous skin effect (ASE).

II. EXPERIMENT

All the CESR measurements reported here have been made with an X-band electron paramagnetic resonance spectrometer. Magnetic-field modulation was applied with modulation frequency 10^5 Hz. The temperature was changed from 10 to 300 K.

The sample was put in the middle of a cavity that is into the point of the maximum magnetic component of the microwave field. The change of the modulation field amplitude does not affect the signal shape but results in the proportional growth of the signal amplitude.

The CESR was observed for the nitrogen and carbon austenites. Characteristics of the samples are given in Table I. Measurements were made on samples with plastic deformation (marked "+" in Table I) and samples annealed after the deformation (those which produced the CESR signal are marked "○" in Table I). The samples with the plastic deformation are foils taken after the rolling of a steel ribbon. The samples were subsequently annealed for 30 min at the temperature 1100 °C followed by hardening in water or oil. The size of the plates in the cavity was 2 mm×20 mm for all samples, the thickness of the plates is shown in Table I. The temperature was measured with the germanium thermometer.

Figure 1 illustrates CESR signals recorded on the temperature $T=39$ K for samples N1 and C3. Signals were recorded at every 5 K interval. Then we measured the
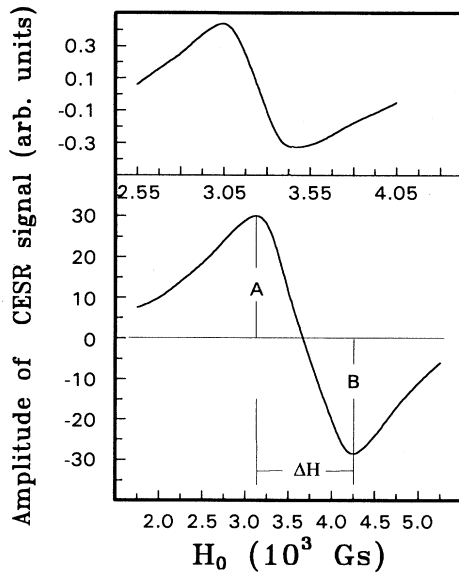
FIG. 1. CESR signals for samples C3 (a) and N1 (b); $T=39$ K; curve (b) illustrates specifications adopted in the text: ΔH, "peak-to-peak" linewidth; $R = |A/B|$, asymmetry parameter.

signal amplitude A in the maximum and B in the minimum of the resonance signal (see Fig. 1), the "peak-to-peak" signal width ΔH in the units of the magnetic field H_0. Temperature curves were constructed for values $I(T)=(|A|+|B|)(\Delta H)^2$, $\Delta H(T)$ and for asymmetry parameter $R(T)=|A/B|$. The combination of these dependencies enables to be confident that we are dealing with the CESR signal and to determine the values of the skin layer depth δ and the electron diffusion length δ_e.

The value $I(T)$ in analogous to the integral intensity of the derivative absorption signal. As for the localized paramagnetic centers the change of the $I(T)$ is proportional to the change of the paramagnetic centers content.

TABLE I. Sample characteristics.

Number of sample	Content of alloy	Concentration of interstitial mixture, at. %		Thickness of sample (μm)
		nitrogen	carbon	
N1	$Cr_{21}Ni_{16}Mn_7$	0.51 (+)		70
N2		0.94 (0,+)		40
N3		1.4 (0,+)		70
N4		1.5 (+)		70
C1	$Cr_{20}Ni_{16}Mn_{16}$		0.28 (+)	60
C2			0.52 (+)	50
C3			0.66 (+)	60

It is not as simple for the CESR because the signal shape is changing during the temperature change.

Experimental points for $I(T)$, $\Delta H(T)$, and $R(T)$ are presented in Figs. 2, 3, and 4 for carbon (a) and nitrogen (b) austenites. The experimental conditions such as the modulation amplitude, the microwave field intensity, and the amplification coefficient are kept unchanged in the measurement process.

The annealed samples normally gave no CESR signal. Samples N2 and N3 were an exception. For the other samples the observation of the CESR is linked to the existence of deformations. There is a more or less narrow temperature interval where the CESR could be studied for each sample. The nitrogen austenite samples have this interval at lower temperatures as compared with the carbon austenite. The temperature interval of the intensive CESR in the deformed samples is broader than in the annealed samples. Some of the annealed samples were hammered, after which they produced the CESR signal with properties similar to those in the deformed samples. The increase of the surface impedance of the electropolished copper sample after mechanical polishing was reported earlier in Ref. 14. We noticed that the CESR signal shape acquires greater symmetry at large degrees of
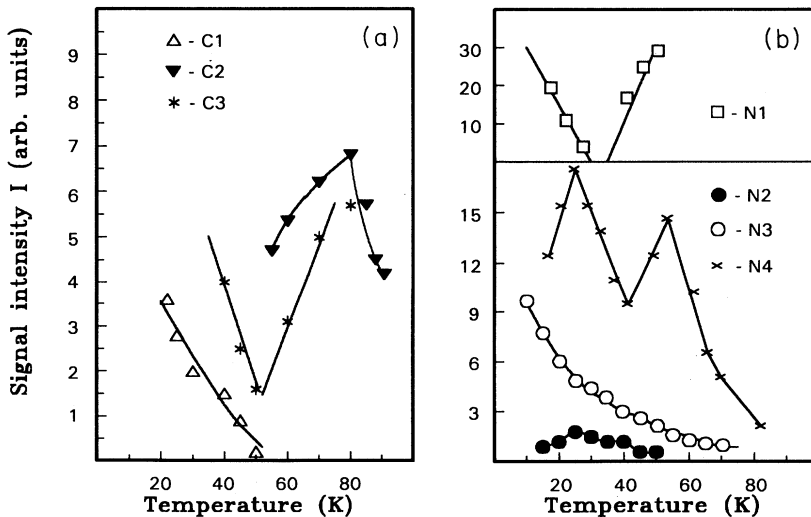

FIG. 2. The signal intensity $I=(|A|+|B|)(\Delta H)^2$ vs temperature for carbonic (a) and nitrogen (b) austenite samples in arbitrary units: points, experimental data; lines, theoretical curves $I(w)$.
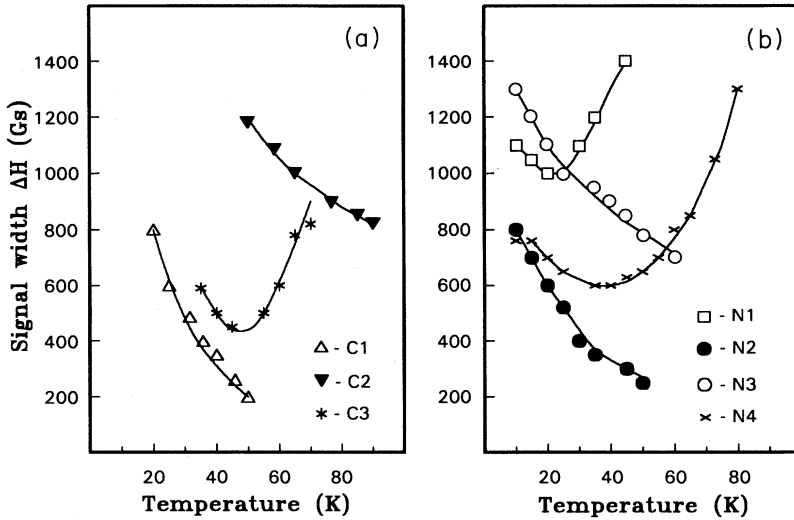
FIG. 3. Temperature dependence of the linewidth "peak-to-peak" for carbonic (a) and nitrogen (b) austenite samples: points, experimental data; lines, computed through (A1)–(A8) theoretical curves $h(w) = \Delta H T_S$.

deformation.

The experimental spectral lines are rather broad. This is caused by the large probability of spin scattering on the magnetic inhomogeneities and the electron exchange interaction.[7,21] If the electron cyclotron frequency ω_c and the time between electron collisions τ are such that $\omega_c \tau$ is comparable to 1, the diffusion coefficient becomes anisotropic,[21]

$$\delta_e^2 = \delta_{e0}^2 \left[\frac{\sin^2\theta}{\omega_c^2 \tau^2 + 1} + \cos^2\theta \right] .$$

θ is the angle between the directions of the magnetic field H_0 and of the normal to the sample plain n. In this case we should observe the same law for the signal width change during the turn of field H_0 from $H_0\|n$ to $H_0 \perp n$. Figure 5 shows this change for sample N2 and we found its $\omega_c \tau = 0.25$. This effect is small for the other samples as well.

III. THEORY OF CESR IN ALLOYS

The power of the microwave field $H_1(t)$ absorbed by the metal sample in the middle of a cavity with the wave type H_{011} is

$$P = \left[\frac{c}{4\pi} \right]^2 H_1^2 \mathrm{Re}(Z) , \tag{1}$$

with H as the field amplitude at the surface of the sample and Z as the surface impedance. If the external static magnetic field H_0 is applied, the impedance Z may be presented as

$$Z = Z_0 (1 + \chi_{0S} G) , \tag{2}$$

with Z_0 as the spinless surface impedance, G is a function characterizing the resonance absorption, χ_{0S} is the paramagnetic electron susceptibility
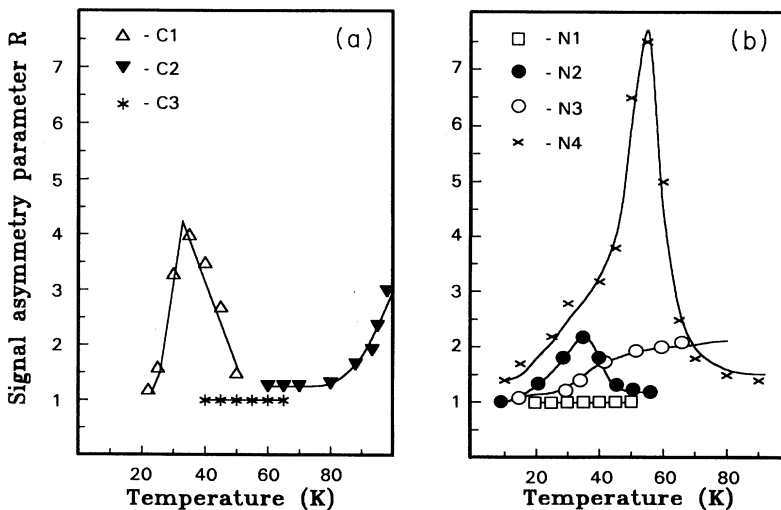

FIG. 4. Temperature dependence of the asymmetry parameter $R = |A/B|$ for carbonic (a) and nitrogen (b) austenite samples: points, experimental data; lines, computed through (A1)–(A8) theoretical curves $R(w)$.
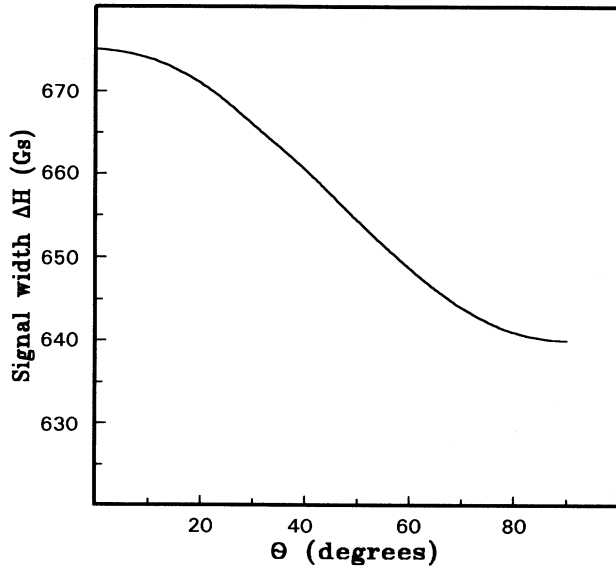
FIG. 5. Linewidth ΔH vs the angle between H_0 and normal to the sample's plain n: $\theta = 0°$ corresponds $H\|n$; sample N2; $T = 30$ K.

$$\chi_{0S} = \tfrac{1}{2} g^2 \mu_B^2 D(\varepsilon_F) , \qquad (3)$$

g is the spectroscopic splitting factor, μ_B is the electron magnetic moment, and $D(\varepsilon_F)$ is the electron-state density on the Fermi surface.

The theory of the CESR signal shape[5] was specified in Refs. 6–10 for different aspects, such as the influence of the electron diffusion, the effects of the spin-wave excitation and others. The correspondence of the theory to the experiment was proven on pure metal samples in Refs. 10 and 11.

The magnetic and electrical fields H,E in the metal foils are the solution of the Maxwell equations and the kinetic equation for the magnetic moment with the diffusion term[8,12] in the sample

$$\mathbf{M} = -g\mu_B [\mathbf{M} \times \mathbf{H}] - \frac{\mathbf{M} - \mathbf{M}_0}{T_s} + D\nabla^2 \mathbf{M} ,$$

$$\nabla \times \mathbf{E} = i\omega c^{-1}(\mathbf{H} + 4\pi\mathbf{M}) , \qquad (4)$$

$$\nabla \times \mathbf{H} = 4\pi\sigma_0 c^{-1} \mathbf{E} ,$$

ω is the microwave frequency, D is the diffusion coefficient, T_S is the electron-spin-relaxation time, and σ_0 is the sample's conductivity. The boundary conditions are determined by the geometry of the sample and the cavity,

$$H\left[\pm \frac{d}{2} \right] = H_1; \quad \frac{d}{dz}(\mathbf{M} - \chi_{0S}\mathbf{H})_{\pm d/2} = \mathbf{0} , \qquad (5)$$

with the thickness of the sample d, and the axis z to the sample plain normal.

As a result of the solution of (4) and (5) the field in the sample is a combination of waves with two wave vectors

K_{10} and K_{20}:

$$K_{10}^2 = i\frac{\delta_e^2}{\delta^2}; \quad K_{20}^2 = 1 + i(\omega - \omega_0)T_S ;$$

$$\delta_e^2 = 2DT_s; \quad \delta^2 = \frac{c^2}{2\pi\delta_0\omega} . \qquad (6)$$

ω_0 is the resonant frequency of the electron spin in field H_0, δ is the "classic" skin layer depth in the sample with the conductivity σ_0, δ_e is the electron diffusion length equal to the path, which the electron covers during the period of spin relaxation T_S and H_0 is the external static magnetic field, $H_0 \perp H_1$.

The above occurs as long as conductivity σ_0 is a local scalar magnitude (the "classic skin effect"). The electron mean free path ℓ is small in alloys particularly in the sample with plastic deformation. However, the skin layer depth δ could get smaller than ℓ when the temperature is down. For this reason we can have conditions of the classic skin effect as well as the ASE conditions, since the CESR measurements are made within the wide temperature range.

If the ASE occurs, the conductivity becomes nonlocal.[17-19]

Assuming nonlocal conductivity $\sigma_{xx}(K) = j_x(K)/E_x(K)$ let us insert it into the system Eqs. (4) and (5). According to theory[20]

$$\sigma(K) = \frac{3\arctan(LK)}{2LK}\sigma_0; \quad L = \frac{\ell}{\delta_e} , \qquad (7)$$

where σ_0 is conductivity with no account of its nonlocality and L is the electron free running length.

The substitution of (7) in (4) and (5) and the subsequent solution leads to the fact that the main formula for the complex impedance Z stays the same as that obtained in Ref. 10, but K_{10}^2 and K_{20}^2 are the solutions of the next equation:

$$[1 + i(\omega - \omega_0)T_S - K^2]\left[K^2 - i\frac{\delta_e^2}{\delta^2}\frac{\arctan(LK)}{LK} \right] = 0 . \qquad (8)$$

Thus, K_{20} is unchanged while K_{10} changes not only its value, but ends up with differing real and imaginary parts. In the case of the ASE limit, when $\arctan(LK) = \pi/2$, K_{10} is

$$K_{10} = \tfrac{1}{2}(1 + i\sqrt{3})(\delta_e^2/\delta^2\ell)^{1/3} . \qquad (9)$$

When the temperature grows, the transition from the ASE to the classic skin effect expresses itself in the fact that K_{10} changes from the value (9) to K_{10} in (6). This leads to the change of the Re(Z) and Im(Z) relation and to the change of the CESR signal shape if K_{10} and K_{20} are comparable.

Using formulas (1) for P and the formula for Z obtained in Ref. 10 we received the next theoretical equation for the value $I(\omega) = dP/dH(\Delta H)^2$, which is recorded in the experiment

$$I(x)=8H_1^2 d\omega^2\chi_{0S} h^2(w_0/u_0)^2\frac{d}{dx}G(u,w,x), \quad x=(\omega-\omega_0)T_S; \quad w_0=d\delta_e^{-1}; \quad u_0=d\delta^{-1}; \quad h=\Delta H T_S \ ,$$

$$u=u'+iu''; \quad u'=K_{10}d\delta_e^{-1}; \quad u''=K_{10}d\delta_e^{-1}; \quad w=w'+iw''; \quad w'=\frac{w_0}{\sqrt{2}}[(1+x^2)^{1/2}+1]^{1/2} \ ,$$

$$w''=\mathrm{sgn}(x)\frac{w_0}{\sqrt{2}}[(1+x^2)^{1/2}-1]^{1/2} \ .$$

The formulas for $G(u,w,x)$, which were used for the computer calculation, are given in the Appendix. When $u'=u''$, it agrees with those from Ref. 10. Let us put down $I(x)$ as $I(x)=I_0\chi_{0S}F(w,u,x)$, where I_0 depends only on experimental conditions (H_1,ω,d), χ_{0S} is given in (3), and the shape function

$$F(w,u,x)=(hw_0/u_0)^2(d/dx)G(u,w,x)$$

was calculated on a computer. If the experimental conditions (I_0) are kept constant in the course of measurement, the value χ_{0S} [and $D(\varepsilon_F)$ from (2)] can be obtained for each sample from Table I through the fitting of the theoretical and the experimental signal amplitudes $I=|A|+|B|$. This procedure requires knowledge of the values of u_0, w_0. The measurements of temperature dependencies for $I(T)$, $R(T)$, and $\Delta H(T)$ provide a sufficient amount of experimental data to determine the values of u_0,w_0.

The procedure is as follows. Using the computer we find the positions of $F(w,u,x)$ extrema x_{max}, x_{min} and the values F_{max}, F_{min}, $h=(x_{max}-x_{min})=T_S\Delta H$, $I=h^2(|F_{max}| +|F_{min}|)$, and $R=F_{max}/F_{min}$ for a large range of u, w values. Temperature dependencies of I, R, and $h=T_S\Delta H$ are determined only through u and w temperature dependencies as T_S doesn't depend on the temperature in deformed samples. The temperature interval where the CESR is observed is narrow for most of the foils (samples N3 and N4 are an exception). Since $u(T)$ changes as $T^{-1/2}$ for the classic skin effect and $u(T)=$constant for the ASE conditions, the temperature dependencies of all the signal parameters are determined mainly through $w(T)$. This fact makes it easy to find $w(T)$.

In earlier papers[9,10] theoretical analysis of the CESR shape deals with obtaining $R=|A/B|$ as the function of

u when (δ/δ_e) is assumed to be constant[10] or $R=|A/B|$ as the function of (δ/δ_e) when u is constant.[11]

Under experimental conditions the CESR signal shape more extensively depends on w and w_0/u_0 (δ/δ_e) changes more quickly than u_0 at the change of temperature. On the other hand the smooth dependence $R(\delta/\delta_e)$ corresponds to the dependence $R(w)$ only for $w\ll1$, $u\gg1$, when $I(x)$ does not depend on u. We cannot consider $w\ll1$ for the deformed foils, and the experimental curves $R(T)$ show that $w\geq1$. For this reason we relied on the calculated dependencies $R(w)$, $\Delta H(w)$, and $I(w)$ at different values $\beta=w_0u_0$ remaining fixed. In accordance with the definition δ and δ_e we have $w_0\propto\ell^{-1/2}$, $u_0\propto\ell^{1/2}$, where ℓ is the electron mean free path so that $\beta(T)$ is constant under the classical skin effect. If the ASE occurs, $\beta(T)$ is proportional to $w(T)$.

We have illustrated the calculated $I(w)$, $R(w)$, and $h(w)=T_S\Delta H$ on Fig. 6 at $\beta=20$ and $\beta=40$ for the classic skin-effect conditions. We can see that the curves $I(w)$, $R(w)$, and $h(w)$ look like $I(T)$, $R(T)$, and $\Delta H(T)$ on Figs. 2, 3, and 4.

The same curves for $\beta=20$, taking the ASE into account are shown on Fig. 6 by dashed lines, to compare with those without the ASE (solid lines). The ASE leads to the decrease of the spectral line intensity, while the linewidth increases, the minimum of $h(w)$ disappears and the line becomes less asymmetrical. The curve $R(w)$ has a single peak with the value $R\leq3$. The interval of w values where $R(w)=1$ spreads out when β increases.

We see that the small values of R and the monotonous decrease of the spectral linewidth are the result of the ASE. The curve $h(w)$ reflects the change of the signal shape and corresponds to the experimental $\Delta H(T)$ as long as the spin-relaxation time T_S does not depend on the temperature. The temperature widening of the line leads to the disagreement of $h(w)$ and $\Delta H(T)$ at high
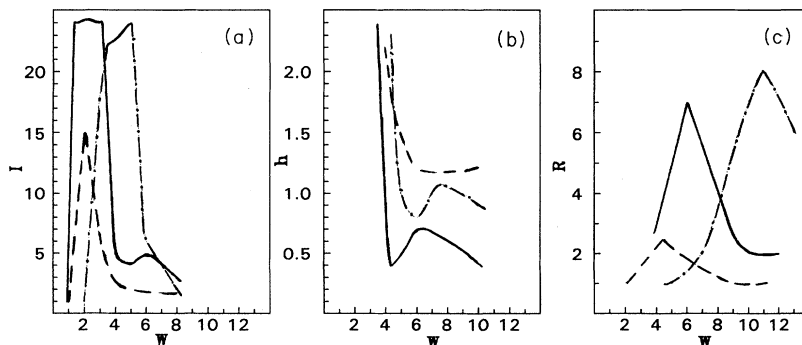

FIG. 6. Computed through (A1)–(A8) theoretical curves: (a) $I(w)$; (b) $R(w)$; (c) $h(w)=\Delta H T_S$; dashed lines—the ASE occurs, $\beta=20$; solid lines—the ASE is absent, $\beta=20$; dot-and-dashed lines—the ASE is absent $\beta=40$.

temperatures. The latter is observed for samples N4 and C3.

IV. COMPARISON OF THEORETICAL RESULTS WITH EXPERIMENTAL EVIDENCE

The curves $I(w)$, $R(w)$, and $h(w)$ fitted with the experiment are shown in Figs. 2, 3, and 4 with dashed lines. The fitting was made on the temperature and w interval width with $I \neq 0$, as well as in peak positions $I(T)$, $R(T)$, $I(w)$, and $R(w)$. Values w, β received from this fitting were checked through the comparison of $\Delta H(T)$ and $h(w)$. We can see in Figs. 2, 3, and 4 that the calculated curves are analogous to the change of the corresponding experimental values with the growth of temperature. For all the samples we found $w = w_0(T^*)\sqrt{T/T^*}$. Values β, u, w, and δ, δ_e found from the fitting of the theoretical and experimental curves and temperature corresponding to these values are given in Table II for all of samples.

The CESR signal was not observed for the initial annealed sample N1. An intensive signal with large linewidth appeared after the mechanical treatment of the sample surface. The signal shape properties show that the ASE is essential. That is why $R = 1$, ΔH is large, and the signal is observed at the narrow temperature interval. This makes the results of the curves fitting for N1 rather doubtful.

The low value R and the smooth decrease of the line width give the evidence for the ASE in samples N2, N3, C1, and C2. For samples N3 and N4 the signal is observed at a wider temperature interval, and the significance of the ASE drops at $T > 50$ K. That is why R begins to increase at lower values T, which would not occur under the ASE. $R(T)$ for the sample N4 reaches the value $R = 7$, which is typical of $R(w)$ under the conditions of the classic skin effect. The curve $I(T)$ for N4 has two peaks. One of them is reached under the conditions of the ASE at $w < 2$, the second peak corresponds to the maximal value of $I(w)$ without the ASE at $w = 4$. The same situation occurs for samples C3 and N1.

Samples of carbonic austenite give signals less intensive but with the same value of the linewidth as the nitrogen austenite signals. The asymmetry parameter R is small as it must be in accordance with $R(w)$ under the ASE conditions.

If we know u, w on the temperature T^*, we have

$$D(\varepsilon_F) = \frac{I_0}{g^2 \mu_B^2} \frac{I_{exp}}{I_{th}} , \tag{11}$$

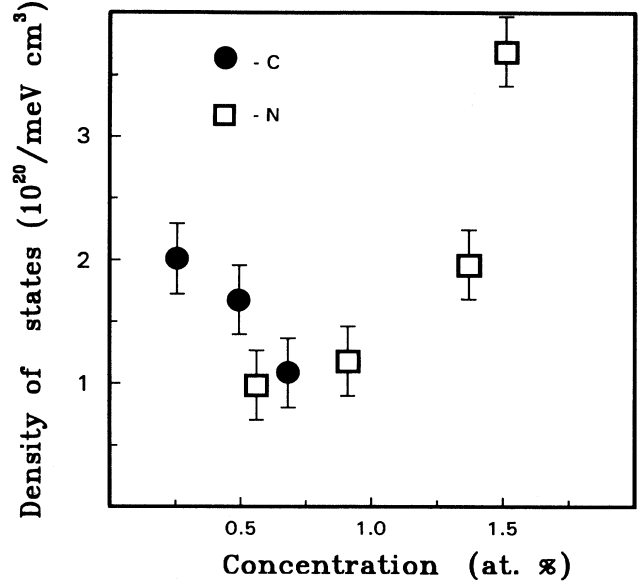FIG. 7. Electron-state density on the Fermi surface vs dopant's concentrations N_i ($i = C, N$): ($\bullet$) carbonic austenite samples; ($\square$) nitrogen austenite samples.

where I_{exp}, I_{th} are the amplitudes of the experimental and theoretical signals on T^*. Since the constant I_0 does not depend on the sample properties, Eq. (11) permits one to find the dependence $D(\varepsilon_F)$ on the nitrogen and carbon concentration at the same temperature. Using MgO:Mn with $N_{Mn} = 6.10^{16}$ cm^{-3} as a reference sample, we have done quantitative estimation of $D(\varepsilon_F)$. Figure 7 shows this dependence for nitrogen (points "$\square$") and carbon (points "$\bullet$") austenite. As we can see from Fig. 7 the electron-state density on the Fermi surface in carbon austenite is lesser than in nitrogen austenite for samples doped with concentrations ≤ 1.5 at % $D(\varepsilon_F)$ increases with the growth of N_N but decreases with the growth of N_C. This result agrees with the fact that the annealed samples of carbon austenite do not produce the CESR signal. Distortions in the sample result in the decrease of the electron diffusion length, the increase of the value w, and the intensification of absorption. The CESR signal is observed only in the narrow temperature interval where values w_0 and u_0 are comparable. In theory the asymmetry parameter of the CESR $|A/B|$ reaches its limit

TABLE II. Parameter β, u_0, w_0, and values of δ, δ_e as a result of the curves fitting on Figs. 2, 3, and 4. T^* is the temperature being corresponded to δ, δ_e.

Sample	T^*, K	β	w_0	u_0	δ, cm	δ_e, cm
N1	20	5	1	5	1.5×10^{-3}	7.0×10^{-3}
N2	15	40	4	10	4.0×10^{-4}	1.0×10^{-3}
N3	15	20	3	7	1.0×10^{-3}	2.3×10^{-3}
N4	20	10	2	5	1.5×10^{-3}	3.5×10^{-3}
C1	20	80	8	10	6.0×10^{-3}	7.8×10^{-4}
C2	80	10	4	2.5	2.0×10^{-3}	1.2×10^{-3}
C3	50	50	4	10	6.8×10^{-4}	1.5×10^{-3}

value 8 (Ref. 11) at low temperatures when $w \ll 1$. This value is not always achieved in experiment, since at low temperatures the ASE causes the signal intensity to decrease.

V. CONCLUSION

It follows from this study that CESR observation in iron-based alloys requires plastic deformation of the samples. There is a narrow interval of d/δ_e values where conduction electrons produce an intensive CESR signal. These values are achieved through the plastic deformation of the alloy samples.

The temperature dependence of the CESR line shape in the austenites is determined by the temperature dependence of the electron diffusion length δ_e during the spin-relaxation time. The CESR occurs under the conditions of the ASE.

We discovered that the electron-state density on the Fermi surface in the carbon austenite samples is less compared with nitrogen austenite. The increase of the nitrogen content in austenite results in the growth of the states density $D(\varepsilon_F)$, while the $D(\varepsilon_F)$ decreases with the growth of the carbon content.

APPENDIX

The CESR signal shape function is equal to

$$F(u,w,x)=h^2(w_0/u_0)^2[dG(u,w,x)/dx] , \tag{A1}$$

$$G(u,w,x)=F_1+F_2+F_3 , \tag{A2}$$

$$F_1=\frac{\kappa_1 v_2 + \kappa_2 v_1}{v_1^2 + v_2^2} , \tag{A3}$$

$$F_2=\frac{2}{u_0^2}\frac{\kappa_3 v_2 + \kappa_4 v_1}{v_1^2 + v_2^2}+2\frac{\kappa_4(v_1^2-v_2^2)+2\kappa_3 v_1 v_2}{(v_1^2+v_2^2)^2} , \tag{A4}$$

$$
\begin{aligned}
F_3=&-2[\cosh(2w')+\cos(2w'')]\\
&\times\{f_1(x)[\kappa_0(v_1^2-v_2^2)+2vv_1v_2]\\
&+f_2(x)[v(v_1^2-v_1^2)-2\kappa_0 v_1 v_2]\}\\
&\times(v_1^2+v_1^2)^{-2} .
\end{aligned}
\tag{A5}
$$

The resonance signal shape is described through f_1, f_2, v_1, and v_2:

$$
\begin{aligned}
v_1(x)&=1-\frac{(u'^2-u''^2)(w'^2-w''^2)+4u'u''w'w''}{(u'^2+u''^2)^2} ,\\
v_2(x)&=2\frac{(u'^2-u''^2)w'w''-u'u''(w'^2-w''^2)}{(u'^2+u''^2)^2} ,\\
f_1(x)&=\frac{w'\sinh(2w')-w''\sin(2w'')}{[w'\sin(2w'')+w''\sinh(2w')]^2+[w''\sin(2w'')-w'\sinh(2w')]^2} ,\\
f_2(x)&=\frac{w'\sin(2w'')+w''\sinh(2w')}{[w'\sin(2w'')+w''\sinh(2w')]^2+[w''\sin(2w'')-w'\sinh(2w')]^2} ;
\end{aligned}
$$

(A6)

(A7)

Coefficients κ_0, κ_1, κ_2, κ_3, and κ_4 are as follows:

$$
\begin{aligned}
&\kappa_1=\frac{1+\cos(2u'')\cosh(2u')}{[\cosh(2u')+\cos(2u'')]^2}; \quad \kappa_2=-\frac{\sinh(2u')\sin(2u'')}{[\cosh(2u')+\cos(2u'')]^2}; \quad \kappa_3=\frac{u'\sin(2u'')-u''\sinh(2u')}{\cosh(2u')+\cos(2u'')} ,\\
&\kappa_4=\frac{u''\sin(2u'')+u'\sinh(2u')}{\cosh(2u')+\cos(2u'')}; \quad \kappa_0=-2\kappa_2; \quad v=\frac{\sin^2(2u'')-\sinh^2(2u')}{[\cosh(2u')+\cos(2u'')]^2} .
\end{aligned}
\tag{A8}
$$

In the case of the classical skin effect $u'=u''=u_0/\sqrt{2}$ and in the case of the ASE $u'=(1/2)u_0(\delta/\ell)^{1/3}$, $u''=(\sqrt{3}/2)u_0(\delta/\ell)^{1/3}$, in other cases u',u'' were calculated from (8) and (10).

[1]V. G. Gavriljuk and S. P. Jefimenko, in *Proceedings of the Second International Conference on High Nitrogen Steel, 1990*, edited by G. Stein and H. Witulski (Stahl und Eisen, Düsseldorf, 1990), pp. 11–21.

[2]V. G. Gavriljuk, V. M. Nadutov, and O. V. Gladun, Fiz. Met. Metalloved. No. 3, 128 (1990) [Phys. Met. Metallogr. (USSR) 69, No. 3, 129 (1990)].

[3]M. Fujikura and K. Takada, Trans. Iron. Steel Inst. Jpn. 15, 469 (1975).

[4]P. Ju. Volosevich, V. N. Gridnev, and Ju. N. Petroff, Fiz. Met. Metalloved. 40, 554 (1975).

[5]F. Dyson, Phys. Rev. 98, 349 (1955).

[6]J. I. Kaplan, Phys. Rev. 115, 575 (1959).

[7]P. M. Platzman and P. A. Wolf, Phys. Rev. Lett. 18, 280 (1967).

[8]M. B. Walker, Can. J. Phys. 48, 111 (1970).

[9]J. H. Pifer and R. T. Longo, Phys. Rev. B 4, 3797 (1971).

[10]J. H. Pifer and R. Magno, Phys. Rev. B 3, 663 (1971).

[11]G. Feher and A. F. Kip, Phys. Rev. 98, 337 (1955).

[12]J. Winter, *Magnetic Resonance in Metals* (Clarendon, Oxford, 1971).

[13]S. Shultz, M. R. Shanaberger, and P. M. Platzman, Phys. Rev. Lett. 19, 719 (1967).

[14]R. G. Chambers, Proc. R. Soc. London, Ser. A 215, 481 (1952).

[15]N. P. Baran *et al.*, Fiz. Met. Metalloved. No. 10, 93 (1990)

[Phys. Met. Mettalogr. (USSR) **70**, No. 4, 88 (1990)].

[16]V. G. Gavriljuk, N. P. Baran *et al.*, Metallofizika **13**, No. 8, 11 (1991) [Sov. Phys. Met. **11**, No. 8, 993 (1993)].

[17]M. Ja. Azbel, V. M. Gerasimenko, and I. M. Lifshitz, Zh. Eksp. Teor. Fiz. **32**, 1212 (1957) [Sov. Phys. JETP **5**, 986 (1957)].

[18]D. C. Mattis and J. Bardeen, Phys. Rev. **111**, 412 (1958).

[19]M. Lampe and P. M. Platzman, Phys. Rev. **150**, 340 (1966).

[20]G. E. Reuter and E. H. Sondheimer, Proc. R. Soc. London Ser. A **195**, 336 (1948).

[21]R. M. White, *Quantum Theory of Magnetism* (McGraw-Hill, New York, 1970).